

Practical considerations for quantitative light sheet fluorescence microscopy

Received: 14 February 2022

Accepted: 31 August 2022

Published online: 20 October 2022

 Check for updates

Chad M. Hobson¹, Min Guo^{2,3}, Harshad D. Vishwasrao⁴, Yicong Wu³,
Hari Shroff^{3,4,5} and Teng-Leong Chew¹✉

Fluorescence microscopy has evolved from a purely observational tool to a platform for quantitative, hypothesis-driven research. As such, the demand for faster and less phototoxic imaging modalities has spurred a rapid growth in light sheet fluorescence microscopy (LSFM). By restricting the excitation to a thin plane, LSFM reduces the overall light dose to a specimen while simultaneously improving image contrast. However, the defining characteristics of light sheet microscopes subsequently warrant unique considerations in their use for quantitative experiments. In this Perspective, we outline many of the pitfalls in LSFM that can compromise analysis and confound interpretation. Moreover, we offer guidance in addressing these caveats when possible. In doing so, we hope to provide a useful resource for life scientists seeking to adopt LSFM to quantitatively address complex biological hypotheses.

Fluorescence microscopy is an essential tool that facilitates observations of intricate and often dynamic biological processes. Beyond their observational use, fluorescence microscopes are increasingly appreciated as desirable means of pursuing quantitative, hypothesis-driven research^{1–3}. As such, recent years have witnessed a boom in microscopy technology development, pushing the boundaries of spatial resolution, acquisition speed, imaging depth and biocompatibility^{4–11}. Of particular interest to many biologists is a subset of these technologies known as light sheet fluorescence microscopy (LSFM). As has been previously reviewed^{5,12–16}, there exist a myriad of light sheet microscopes, each often tailored toward a specific application. The core principle, however, remains the same: by illuminating a thin slice of the sample on the image plane, both out-of-focus fluorescence and overall irradiation of the specimen are substantially reduced^{17,18}. Moreover, the gamut of light sheet microscopes spans multiple biological length scales^{19,20}, making it an attractive imaging technique for cell and developmental biologists alike. LSFM thus enables researchers to rapidly observe and quantitatively assess biological processes and structures in three dimensions with minimal phototoxicity and photobleaching.

As with any quantitative method, however, one must appreciate the underlying caveats and assumptions to ensure accurate and reproducible measurements. Arguably the most glaring caveat in quantitative microscopy is that the brightness and location of pixels in an image are merely estimates of the underlying specimen²¹. Factors inherent to fluorescence microscopy such as diffraction, noise and labeling indicate that the acquired images imperfectly represent the true biological structure. Any downstream quantitative analysis is then subject to this caveat. Although detailed guides can aid researchers in characterizing and potentially correcting for such artifacts in conventional microscopes^{3,21–25}, new imaging modalities—particularly LSFM—often warrant unique considerations.

In this Perspective, we describe various pitfalls in LSFM, and highlight how they can alter and undermine quantitative analysis. Additionally, we provide guidance in recognizing and, when possible, remedying these issues to ensure unbiased and reproducible measurements. By performing experiments on a range of light sheet microscopes, both custom and commercial, we aim to be agnostic to any specific variation of LSFM; rather, we focus on issues central to the principle of LSFM, which are thus applicable to all light sheet systems. Our hope is that this

¹Advanced Imaging Center, Janelia Research Campus, Howard Hughes Medical Institute, Ashburn, VA, USA. ²Present address: State Key Laboratory of Modern Optical Instrumentation, College of Optical Science and Engineering, Zhejiang University, Hangzhou, China. ³Laboratory of High Resolution Optical Imaging, National Institute of Biomedical Imaging and Bioengineering, National Institutes of Health, Bethesda, MD, USA. ⁴Advanced Imaging and Microscopy Resource, National Institutes of Health, Bethesda, MD, USA. ⁵Present address: Janelia Research Campus, Howard Hughes Medical Institute, Ashburn, VA, USA. ✉e-mail: chewt@janelia.hhmi.org

guide will be a useful starting point for those wishing to adopt LSFM as a means of testing complex biological hypotheses, improving their confidence in the quantitative conclusions drawn from such studies.

Light sheet confinement

Light sheet microscopes are often tailored toward specific biological length scales. The first important consideration in quantitative LSFM is then optimizing the size and shape of the light sheet for the given specimen. The illumination in a light sheet microscope is either static (for example, cylindrical lens¹⁷ or spatial light modulator²⁶) or dynamic (for example, digitally scanned beam²⁷ or field synthesis²⁸). In either case, the performance of optical sectioning—that is, the reduction of out-of-focus light—is directly related to the thickness of the light sheet and the distance over which the thickness remains approximately constant, also known as the depth of field (DOF). An ideal light sheet would be as thin as possible and possess a DOF spanning the sample, enabling adequate optical sectioning over the desired field of view (FOV). However, due to the physical principles that underly beam propagation, there is always a tradeoff between light sheet thickness and DOF. In the Gaussian beam approximation, DOF is twice the Rayleigh length, defined as the distance over which the beam radius diverges to a value no larger than $\sqrt{2}$ times the beam waist (Supplementary Fig. 1). This DOF is proportional to the square of the beam waist²⁹, which implies a Gaussian beam with a relatively smaller beam waist produces better optical sectioning at the cost of more rapid divergence and a smaller usable FOV. Although the specific scaling relationships change for high-numerical aperture systems and alternative beam characters^{26,30,31}, the intrinsic tradeoff between light sheet thickness and DOF remains true. Practically speaking, tuning the beam waist (and DOF) may be helpful when imaging samples of different sizes, tailoring the optical sectioning to the desired FOV. There do exist means of circumventing this limitation, most notably through tiling light sheet microscopy³². By sequentially stepping the excitation sheet in the direction of propagation and collecting an image at each light sheet position, the DOF and total FOV can be extended for a given sheet thickness at the cost of reduced imaging speed and increased photobleaching and phototoxicity. The total tiled DOF, however, should still be matched to the length scale of the specimen. Extending this concept to use a tightly focused light sheet scanned through the specimen in its propagation direction in conjunction with a rolling shutter yields axially swept light sheet microscopy^{33–37}. In this instance, the DOF of the sheet is matched to the shutter size, and thus the previous discussion is less applicable.

To demonstrate the value of tuning the beam waist, we used a dual-view inverted selective plane illumination microscopy (diSPIM) system^{38,39} to image living *Caenorhabditis elegans* embryos with all cell membranes labeled by green fluorescent protein (GFP) (Fig. 1). We changed the light sheet beam waist by adjusting an aperture conjugate to the back focal plane of the illumination objective. Since *C. elegans* embryos have a size of roughly 30 μm in the direction of beam propagation, using a beam waist of 1.6 μm (corresponding DOF roughly 30 μm) offers better optical sectioning and image quality (Fig. 1a,b top) than using a beam waist of 3.3 μm (producing a DOF of more than 100 μm , much larger than necessary). The latter choice introduces considerably more out-of-focus contamination, resulting in reduced image contrast (Fig. 1a,b bottom). The degradation in image quality is especially clear when looking at cell membranes in the magnified view (Fig. 1c) and associated line profiles across the cell membranes (Fig. 1d).

Coalignment of the light sheet and focal plane

A key difference between conventional microscopes and light sheet microscopes is that the latter uncouples the illumination and detection pathways, allowing independent control of the light sheet and detection focal plane. Traditional epifluorescence microscopes use the same objective to excite the sample and detect the emitted fluorescence, which usually guarantees that the illumination coincides

with the image plane. Such alignment is not guaranteed in a light sheet microscope. Misalignment between the light sheet position and the detection focal plane can alter both the intensity and position of the emitted fluorescence, which can confound downstream quantitative measurements.

Light sheet misalignment can occur in several ways, including an offset or a relative tilt between the light sheet and the image plane (Fig. 2a). One of the most disruptive effects of such misalignments is a dramatic increase in out-of-focus light and a loss of contrast and resolution. These effects are exacerbated when using high-numerical aperture systems. To demonstrate these effects, we acquired images of HeLa cells fixed and stained with Alexa Fluor 488 Phalloidin using a modified lattice light sheet microscope (LLSM)²⁶ and created maximum intensity projections (MIPs). Offsetting the light sheet from the focal plane by as little as 1 μm highlights a clear degradation of optical sectioning and contrast (Fig. 2b). For further inspection, we calculated the Fourier transform of each MIP (insets in Fig. 2b) and plotted the intensity as a function of radial distance (Fig. 2c). Comparing these plots between the aligned and offset cases shows that misalignment between the light sheet and the focal plane reduces the high frequency content in the image (Fig. 2c). Thus, misalignment can ultimately cause a user to miss fine biological structures at the limit of the microscope's resolving power.

Unfortunately, intensity and contrast are not the only features that can be distorted by improper alignment. Altering the position of the light sheet relative to the image plane can also change the apparent axial position of biological structures. This is particularly important when considering multicolor experiments. As a demonstration, we acquired images of HeLa cells fixed and stained for LAMP1 (green) and transferrin (magenta) (Fig. 2e–g) on an LLSM²⁶. Transferrin is known to localize within lysosomes (LAMP1)⁴⁰, which is accurately observed when each wavelength light sheet is properly aligned both to each other and to the image plane (Fig. 2d,f). However, a slight misalignment between the two excitation wavelengths relative to each other drastically shifts the apparent position of the transferrin outside the lysosomes (Fig. 2e,g). Thus, misalignment can negatively affect three-dimensional (3D) colocalization measurements, particularly for objects with sizes nearing the diffraction limit.

Visual inspection is typically not a reliable means of ensuring proper alignment, particularly when dealing with sparsely labeled specimens. It is therefore crucial to systematically align the light sheet to the focal plane before an experiment. This is most easily done by acquiring point spread function measurements (PSFs); that is, imaging fluorescent beads whose size are below the resolution of the instrument. When the light sheet and focal plane are misaligned, the axial view of the PSF becomes skewed (Supplementary Fig. 2). Coaligining the light sheet to the focal plane subsequently tightens the PSF and returns it to the optimal, symmetric shape (Supplementary Fig. 2). This must be performed independently for each excitation wavelength. If the same settings are used for different light sheet wavelengths, chromatic aberrations and the slightest misalignments between laser lines will cause each wavelength to excite different planes of the specimen. We therefore recommend using multi-spectral fluorescent beads, which allow a user to assess both the alignment of each excitation wavelength as well as the coregistration between channels.

Although we have predominantly focused on the implications of an offset between the light sheet and the image plane, it is also important to ensure that the light sheet is not tilted or rotated relative to the image plane (Fig. 2a). A tilted light sheet can cause similar effects to an offset light sheet, but these artifacts become progressively worse across the FOV. The tilt of the light sheet can be assessed by acquiring PSFs at the edges of the usable FOV. If the PSFs at each edge are skewed in opposite directions, there is a rotation between the light sheet and the image plane (Supplementary Fig. 3). This should be corrected if possible; otherwise, the resulting data must be interpreted with

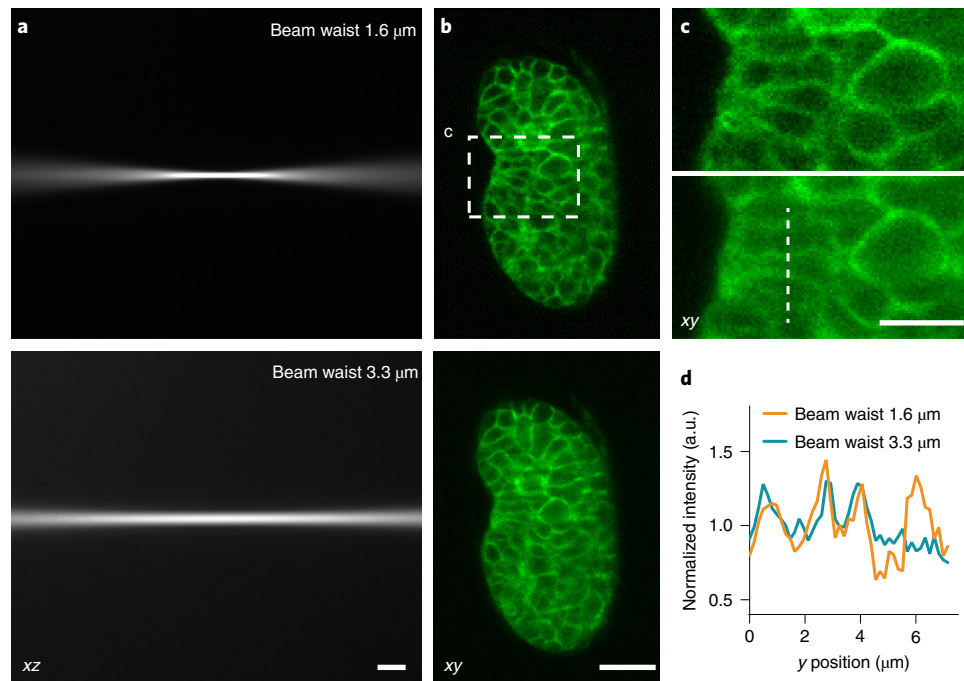


Fig. 1 | Effect of beam waist on image quality. **a**, Gaussian illumination beams in fluorescein solution with different beam waists. The full-widths at half-maximum of the beam waists are estimated as 1.6 (top) and 3.3 (bottom) μm based on the line profiles of these images. **b**, Images of *C. elegans* embryos with cell membrane labeled, corresponding to the illumination beams in **a**. Note the bottom image is more contaminated by out-of-focus fluorescence when using the beam with

3.3 μm waist. **c**, Higher magnification views of the dashed white box in **b**. **d**, Line profiles corresponding to the white dotted line in **c**. Intensities are normalized to the average of each profile. The laser power was adjusted for each case of light sheet thickness to keep the signal to noise roughly the same across images. Scale bars 10 μm in **a** and **b**, and 5 μm in **c**. Data acquired with diSPIM, from one view. a.u., arbitrary units.

this known caveat. Moreover, these corrections should be performed with the microscope equilibrated to the desired imaging temperature. Changes in temperature can alter the light sheet position, thus undoing these calibrations. Additionally, any drift in the system, be it thermal or mechanical, can alter this alignment. These sources of sheet misalignment, along with several others, are summarized in Box 1. Many commercial light sheet microscopes have means of empirically estimating excitation and detection alignment during an experiment, providing an excellent option to maintain alignment over long imaging durations. Given the impact on both the apparent brightness and location of structures within an image, it is important to ensure the system is properly aligned before any quantitative experiment.

FOV uniformity

LSFM is exceptionally useful for rapidly acquiring volumetric images across large FOV. However, there is often an underlying misconception that across the entire FOV, it is possible to precisely estimate the intensity and position of fluorescent molecules. Uneven illumination intensity, light sheet degradation and FOV distortions can, however, dramatically alter both the measured intensity and position of biological structures. Therefore, they must be accounted for when drawing quantitative conclusions.

Flatfield correction

In general, the intensity of emitted light will be directly related to the intensity of the light used to excite the sample⁴¹. Therefore, heterogeneity in the illumination intensity will bias the signal in the detected image, potentially compromising any further quantitative measures. Light sheet fluorescence microscopes are no exception. Any imperfection along the optical path (for example, misalignment, imperfect lenses, dust and so on) can locally alter the excitation profile. Even in perfectly aligned systems, illumination is not guaranteed to be uniform both in the direction the light sheet travels and the transverse directions. Light

sheet systems that make use of rolling shutters during acquisitions^{33,42–46} are particularly susceptible to uneven illumination due to errors in shutter timing, speed and alignment to the beam (Supplementary Fig. 4). To complicate matters further, diffraction and misalignment between laser lines ensure that the illumination profile is not identical for each excitation wavelength. To demonstrate the effects of uneven illumination, we acquired ratiometric images of myosin II regulatory light chain (RLC) to total myosin II in PtK2 cells on an LLSM²⁶ (Fig. 3a). Since RLC is a stable component of the myosin II heterohexamer⁴⁷, a uniform ratio is expected for the entire FOV. However, the noncorrected LLSM ratiometric images show a smooth gradient. Without the a priori knowledge of the underlying biochemistry of nonmuscle myosin II, this may be interpreted as a true biological result. Thus, nonuniform excitation profiles may alter the quantitative metrics derived from LLSM images; accurately correcting for these heterogeneities is necessary for drawing sound quantitative insights.

It is best practice to visualize the illumination profile of the light sheet before beginning each new experiment. The most common means of doing so is by using a diluted solution of fluorescent dye and recording images for each illumination wavelength over the desired FOV (Supplementary Fig. 5). When doing this, it is important that the dye solution is prepared with the same imaging media that will be used for experiments and that the microscope is equilibrated to the correct imaging temperature. Applying a ‘flatfield correction’ is then straightforward (Supplementary Materials and Methods). Fortunately, such an approach works for both single- and multi-photon excitation schemes. As shown in Fig. 3b, applying a flatfield correction to the ratiometric myosin example substantially mitigates the biased ratio along the vertical axis. Examining the illumination profiles in hindsight (Fig. 3c) reveals that the skewed ratios are a result of uneven illumination rather than any underlying biological phenomenon.

While imaging a dye solution is often acceptable for flatfield correction, the resulting images may not always perfectly represent the

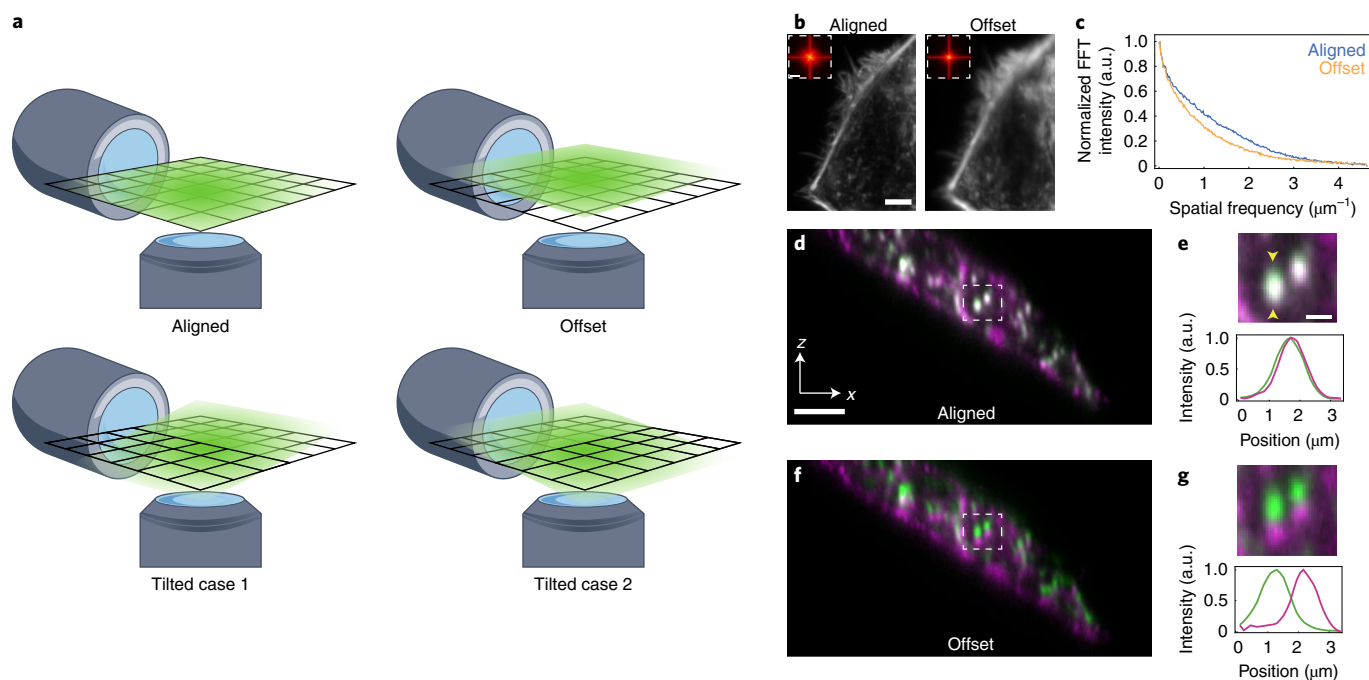


Fig. 2 | Misalignment of light sheet and focal plane compromises feature detection and axial localization. **a**, Schematic representation of misalignments between the light sheet and the image plane. **b**, MIPs from a volumetric image of a HeLa cell fixed and labeled with Alexa Fluor 488 Phalloidin. Images of the same cell with and without a 1 μm offset between the focal plane and the light sheet are shown, displaying degraded resolution and contrast. Insets show a fast Fourier transform (FFT) of the MIPs, scale bar, 2 μm^{-1} . Images were acquired using a modified lattice light sheet microscope. Scale bar, 5 μm . **c**, Radial profile plot of the normalized intensity from the FFT images shown in **b**. The offset profile shows a loss of high spatial frequency features compared to the aligned profile.

d–g, Volumetric images of HeLa cells fixed and stained for LAMP1 (green) and transferrin (magenta) were acquired on a lattice light sheet microscope. **d, f**, A single xz cross section of the same cell is shown wherein the 488 and 561 nm light sheets are coaligned to the focal plane of the detection objective (**d**) and misaligned from the focal plane of the detection objective (**f**) by ± 500 nm, respectively. Scale bar, 5 μm . This light sheet offset causes an apparent axial shift of transferrin outside the lysosomes. **e, g**, An inset of the white dashed box in **d** and **f** as well as a line trace through the left-most lysosome (between yellow arrows) is shown for the coaligned (**e**) and misaligned (**g**) cases. Scale bar, 1 μm .

BOX 1

Common sources of light sheet misalignment

- Mismatched refractive index between media, sample or imaging system
- Change of imaging temperature
- Chromatic shifts
- Mechanical drift
- Temperature and humidity fluctuations
- Strong air currents
- Improper positioning of optics

light sheet profile. Such an image is most appropriate for modeling the central region of the sheet, as only over this region is the thickness of the light sheet similar to the DOF of the detection objective. Outside this region, divergence of the light sheet will excite fluorescent molecules outside the detection plane, potentially altering the image intensity relative to the focused region of the light sheet. Therefore, a flatfield correction based on dye solution images is best used for the central, focused region of the light sheet. While imaging a specimen outside the confocal region is not recommended to begin with,

alternative approaches for flatfield corrections do exist. A potentially more rigorous, yet challenging, approach is to scan a single fluorescent bead incrementally through the FOV, summing the signal at each scan position. The resulting summed signal versus scan position provides a better estimate of the excitation distribution, barring noticeable photobleaching of the fluorescent bead. Finally, if the need for a flatfield correction is realized well after the experimental data have been collected, several approaches exist for retroactively estimating the illumination profile from the raw images themselves^{48–50}. However, such approaches are often most effective for densely labeled specimens as they provide more spatial intensity information from which the excitation distribution may be inferred.

Light sheet degradation

Unfortunately, a light sheet with an ideal profile in a dye solution does not always yield uniform excitation throughout the FOV of a sample. As light propagates further into a specimen, scattering can cause the excitation sheet to rapidly disperse^{17,51}. This is especially true for large, dense and heterogeneous samples such as nonoptically transparent embryos and tissue slices. Therefore, even with a light sheet with uniform excitation and a DOF precisely matched to the specimen will show continually deteriorated optical sectioning as the light sheet propagates through the sample, making quantitative analyses exceedingly difficult.

To demonstrate this effect, we acquired images of a *Drosophila melanogaster* embryo with His2Av-EGFP labeled nuclei on a Zeiss Lightsheet Z.1 (Fig. 4). This commercial light sheet microscope can illuminate the sample sequentially from opposing directions (Fig. 4a). Examining the same slice of the embryo with opposing excitation directions highlights how the optical sectioning is dramatically reduced

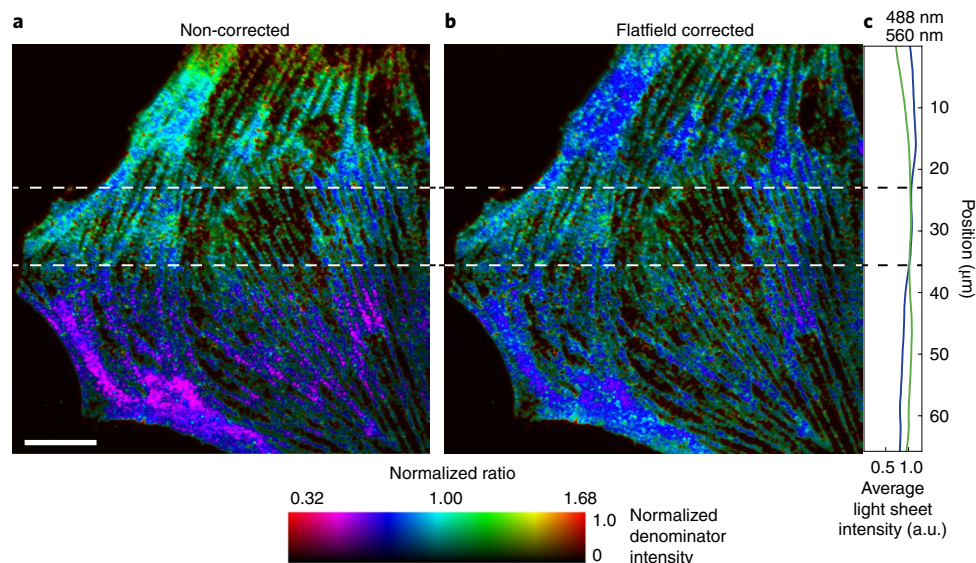


Fig. 3 | Nonuniform illumination intensity in LSFM. Volumetric images of PtK2 cells fixed and stained for myosin RLC (488 nm) and total myosin (560 nm) were acquired on a lattice light sheet microscope. **a, b**, Shown are the intensity-modulated ratiometric images (myosin RLC/total myosin) of the MIPs of these 3D data sets without flatfield correction (**a**) and with flatfield correction (**b**). The flatfield correction was performed for each color before deskewing, projecting and ratioing of the images (Supplementary Fig. 5). **c**, Averaged intensity profile

of the light sheet for each excitation wavelength. The light sheet profiles can be separated into regions (dashed lines) where $I_{488}/I_{560} > 1$ (top), $I_{488}/I_{560} \cong 1$ (middle) and $I_{488}/I_{560} < 1$ (bottom). The implications of these relative illumination intensity changes can be seen in the noncorrected intensity-modulated ratiometric image (**a**) when compared to the flatfield corrected intensity-modulated ratiometric image (**b**). Scale bar, 10 μm .

as the light sheet propagates further into the sample. Moreover, the ability to distinguish a single nucleus from the background on each side of the embryos is entirely changed purely based on the propagation direction of the light sheet (Fig. 4b,c). Unfortunately, this artifact of deteriorated optical sectioning is caused by the specimen itself, thus rendering it more challenging to address than other issues. In some cases, as shown here, systems are equipped with illumination from multiple angles to rectify this effect by fusing together images with complementary excitation directions^{43,51,52}. This fusion and the resulting voxel intensities, however, should be approached cautiously as it may not be immediately obvious how the signal from each raw image contributes to the final fused data set. However, if a light sheet microscope does not have such capabilities, this should be taken as a fundamental limitation around which the experimental design will have to be carefully planned.

Additionally, there exists a second sample-induced artifact for which light sheet microscopes are particularly susceptible. When the excitation sheet encounters a highly scattering or absorbing structure, it ceases to propagate directly behind this object. This results in ‘shadows’ or ‘streaks’ across the image (Supplementary Fig. 6), which can make segmentation particularly challenging across the entire FOV. This artifact and its remedies—such as beam pivoting, Bessel Beam illumination and diffusive optics—have been recently reviewed⁵³, and we refer readers to these resources for a more thorough discussion.

Field distortion

Considerations of FOV uniformity do not end, however, with flatfield corrections and light sheet degradation. LSFM is quickly becoming the modality of choice for imaging cleared and expanded tissue^{37,54–57}. Volume acquisition of such large samples entails acquiring many 3D image subvolumes or ‘tiles’ that overlap their neighbors by some small fraction. To generate the full image volume, neighboring tiles are stitched together by coregistering and fusing their overlap regions. The FOV is selected by the user as a subregion of the camera sensor. There are advantages to using the largest FOV possible (and

thus fewer tiles), such as increased acquisition speed and reduced computational time. The ongoing development of cameras with ever increasing sensor sizes makes it tempting to use the largest FOV camera available. Practically, however, the largest usable FOV is often not determined by the camera, but rather by field-dependent aberrations due to the imaging optics: most commonly the microscope objective. While there are many objectives with excellent aberration correction, light sheet microscopy often imposes constraints that limit objective choice. Specifically, in cleared/expanded tissue imaging, the objective must often tolerate harsh organic solvents with a broad range of refractive indices (1.33–1.56)^{58–65}. To satisfy these requirements, it is unsurprising that objectives sacrifice performance in other areas such as spherical, geometric and chromatic aberration correction. Aberrations must then be carefully considered in the overall experimental workflow.

One of the most common FOV-limiting aberrations is geometric distortion: a change in lateral magnification (increase or decrease) with increasing off-axis distance from the center of the FOV. Geometric distortion is not unusual in complex, compound lens systems and causes the image to appear progressively warped toward its periphery. This distortion is particularly problematic for multi-tile acquisitions as the image periphery is used to coregister and stitch neighboring tiles. To illustrate this effect, we used the full FOV (2,048 × 2,048 pixels) available on a cleared tissue dual-view inverted selective plane illumination microscope to perform a multi-tile acquisition⁵⁵ over a sample of iDISCO cleared brain tissue labeled with TOPRO3. Neighboring tiles were acquired with 15% overlap (Fig. 5a, overlap regions in magenta and cyan). Stitching these tiles together is then a matter of coregistering their overlap regions (Fig. 5b) in 3D. Using the ImageJ Stitching Plugin⁶⁶, which performs 3D coregistration using only translation, we find that the centers of the overlap regions (Fig. 5c) register well. In contrast, the ends of the overlap regions that correspond to the FOV peripheries of the two tiles (Fig. 5d) do not. In the resulting registration, large structures such as nuclei partially overlap, but smaller structures such as nucleoli fail to coregister entirely.

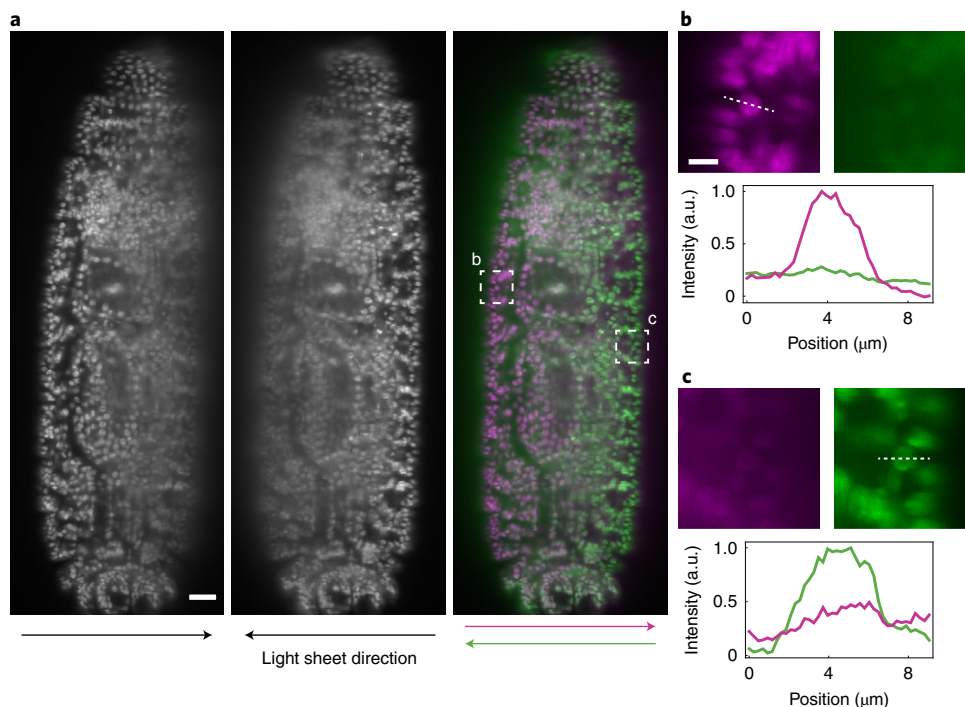


Fig. 4 | Degradation of light sheet quality. **a**, Selected frame from a 3D acquisition of a *D. melanogaster* embryo with His2Av-EGFP labeled nuclei. Images were acquired on a Zeiss Lightsheet Z.1. The same frame was imaged with sequential excitation incident on the embryo from opposing directions, as is indicated by the arrows. Also shown is an overlay of the two images with opposing light sheet propagation directions. As the light sheet propagates further into the

sample, the light sheet confinement degrades, reducing optical sectioning. Scale bar, 20 μm **b,c**, Insets from the accompanying white dashed rectangles shown in **a**; images are pseudocolored to indicate the direction of light sheet propagation. A line trace through a single nucleus shows a dramatic reduction both in overall intensity and contrast when the light sheet must pass through the entire sample. Scale bar, 5 μm .

Since geometric distortion is a function of distance from the FOV center, a straightforward solution is to reduce the FOV. However, this requires more tiles to be acquired, increasing the overall acquisition time (Fig. 5i). In our example, we tried several progressively smaller choices for our FOV, always using 15% overlap. The optimal FOV (1,536 \times 1,536 pixels in this example) (Fig. 5e) is the largest FOV that maintains acceptable coregistration of the overlap regions (Fig. 5f) near their centers (Fig. 5g) and adequate coregistration down to the level of nucleoli at the periphery (Fig. 5h). A larger FOV would show coregistration failure near the periphery, and a smaller FOV did not noticeably improve the uniformity of coregistration but required more tiles. Moreover, it is important to note that for light sheet systems with zoom optics, using a larger FOV through a zoom functionality will still result in field distortions even if the number of pixels is held constant. To quantify the quality of image registration, we used the normalized cross correlation (NCC), which is a measure of both similarity and colocalization (Fig. 5j). When examining the NCC as a function of FOV size, there is a clear transition zone of degraded registration quality with increasing FOV (Fig. 5j). The specific value of the NCC, however, can vary between samples and imaging conditions, and thus a specific threshold cannot be recommended for all experiments. In conclusion, when selecting the FOV size, it is important to consider that a larger FOV may render the peripheral data susceptible to noticeable errors, affecting quantification. We note that field distortion is not unique to the microscope and optics used here, but is common to many light sheet systems. The specific FOV described here, however, is applicable only for this particular light sheet microscope, and we strongly encourage readers to perform their own experiments to determine the ideal balance between FOV size and registration accuracy for their samples.

Postprocessing

To this point, our focus has resided entirely on pitfalls associated with LSFM image acquisition. However, many quantitative analyses performed on LSFM data sets benefit from or even require image processing. At times, these image processing workflows can further confound analysis and interpretation if not performed properly. As has been previously reviewed^{67,68}, image processing is useful and often necessary with any microscopy modality. There are, however, several processing steps commonly associated with LSFM that warrant further examination.

Deconvolution

Every microscope acts as a low pass filter, distorting the size, shape and intensity of fine details in the sample. This is because the true biological structure is convolved with the microscope PSF, resulting in a blurred version of the specimen imaged onto the detector. With knowledge of microscope PSF, however, one can computationally deconvolve these images⁶⁹⁻⁷¹. When implemented properly, deconvolution can yield a more accurate representation of the underlying sample (Supplementary Fig. 7). Deconvolution has become a common processing step in LSFM, often used to reduce blur, increase contrast, facilitate multiview fusion and improve resolution. However, several caveats are important to keep in mind, particularly for quantitative analysis.

A key assumption is that the PSF used in deconvolution accurately represents the PSF of the microscope. Therefore, it is wise to either use an experimentally derived PSF or verify that a theoretical PSF appropriately models the blurring introduced by the microscope. For LSFM, the PSF mainly depends on (1) light sheet thickness, (2) wavelength and (3) alignment. Thus, a new PSF must be used when using a different light sheet, and separate PSFs would ideally be used when deconvolving multi-channel images. A misaligned light sheet system

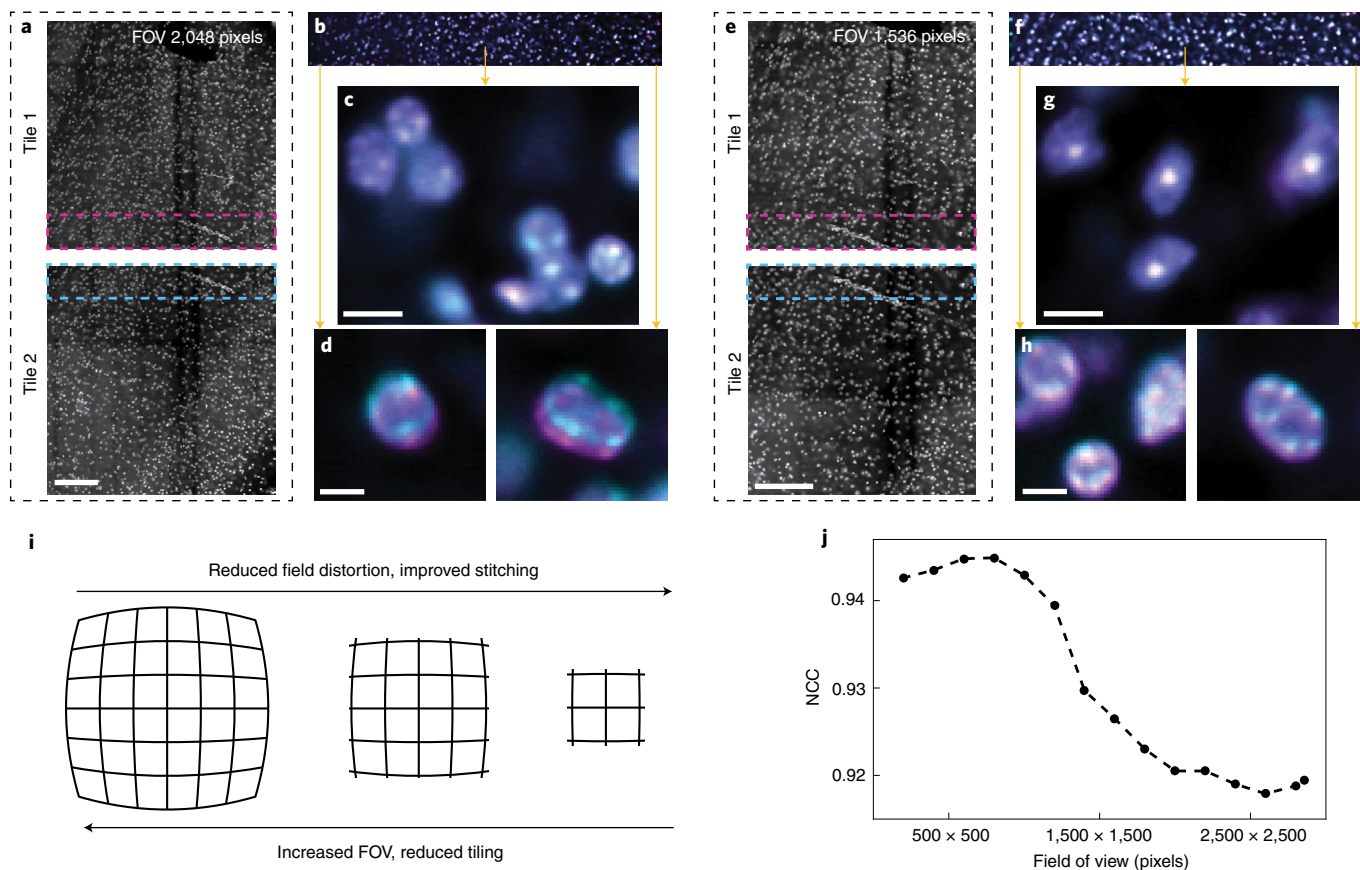


Fig. 5 | Reducing FOV improves accuracy of stitching. **a**, Neighboring tiles acquired with a full FOV (2,048 × 2,048 pixels) and 15% overlap are stitched together by coregistering their overlap regions (magenta and cyan dashed boxes). Scale bar, 100 μm. **b–d**, Coregistration of the overlap regions (**b**; displayed in magenta and cyan) works well near the center of the overlap region (**c**) but degrades toward the periphery (**d**). While larger structures such as nuclei still coregister, small structures (for example, nucleoli) do not, compromising the accuracy of stitching and image quality of the fused overlap

region. **e**, Reducing the FOV (1,536 × 1,536 pixels) clips the warped periphery of the full field. Scale bar, 100 μm. **f–h**, The resulting coregistration of neighboring tiles (**f**) shows better uniformity from the center (**g**) to the periphery (**h**) of the overlap region, ensuring a better stitch and fusion. **i**, Schematic representation of the inherent tradeoffs associated with FOV. Increasing FOV can reduce the need to tile acquisitions, thus increasing speed. Reducing the FOV minimizes field distortion and improves tile stitching accuracy. **j**, NCC for overlapped regions of neighboring tiles shown for varying FOV. Scale bars in **b, d, g, h**, 5 μm.

can be particularly problematic (Supplementary Fig. 7). As we have shown, a misaligned system yields an elongated and asymmetric PSF (Supplementary Fig. 2). Therefore, if an ideal PSF is used to deconvolve an image from a misaligned system, the fundamental assumption of deconvolution is invalidated. The ‘improvements’ to image quality are often marginal compared to data collected with the aligned system and are not guaranteed to accurately represent the underlying structure (Supplementary Fig. 7). A misaligned system is not the only means by which a PSF is no longer accurate. If the DOF of the light sheet does not span the entire specimen or if the light sheet is scattered or aberrated, the PSF varies over the FOV. Similarly, imaging deep into aberrating specimens can cause image distortions not captured by an ideal PSF. Deconvolution in such cases is subpar.

Assuming the PSF is accurate, there are additional considerations for appropriate use of deconvolution. The first is ‘over-deconvolution’. In many cases, deconvolution is an iterative process whereby the user prescribes a set number of times the routine will run. At first it may be tempting to boost the number of iterations under the assumption that more iterations will yield continued improvement. However, too many iterations inevitably lead to artifacts⁷² (for example, noise amplification). We therefore recommend varying the number of iterations to understand the point at which artifacts may be introduced. The second important caveat is that many common deconvolution algorithms do not preserve linearity⁷¹; that is, an object twice as bright

as another before deconvolution may appear three times as bright after deconvolution, for example. Ideally, the assumption of linearity would be checked for the specific deconvolution algorithm used by the user. Otherwise, we do not recommend making intensity-based measurements on deconvolved data sets. Rather, we suggest using the deconvolved data to ease the burden of image segmentation, after which intensity measurements can be performed on the original data. In summary, although deconvolution is a powerful computational tool, its use for quantitative analysis must be approached cautiously given its underlying assumptions, the risk of over-deconvolution and the potential for nonlinear intensity transformations.

Multiview fusion

As shown in Fig. 4, the sample can clearly compromise the integrity of the excitation light sheet. However, aberrating or scattering samples can also reduce detection efficiency, particularly at increasing depths into the sample. One means of compensating for these effects is through imaging a specimen from multiple viewpoints, usually captured by rotating the sample^{73,74} or using multiple detectors arrayed around the specimen^{38,39,51,52,75,76}. If these views are near orthogonal, one gains an additional benefit of improved resolution isotropy^{38,39,73,76}. Multiview imaging, however, requires a modality that is both fast and gentle to minimize photobleaching, phototoxicity and motion blur. Therefore, LSFM is the predominant method of choice^{51,75}.

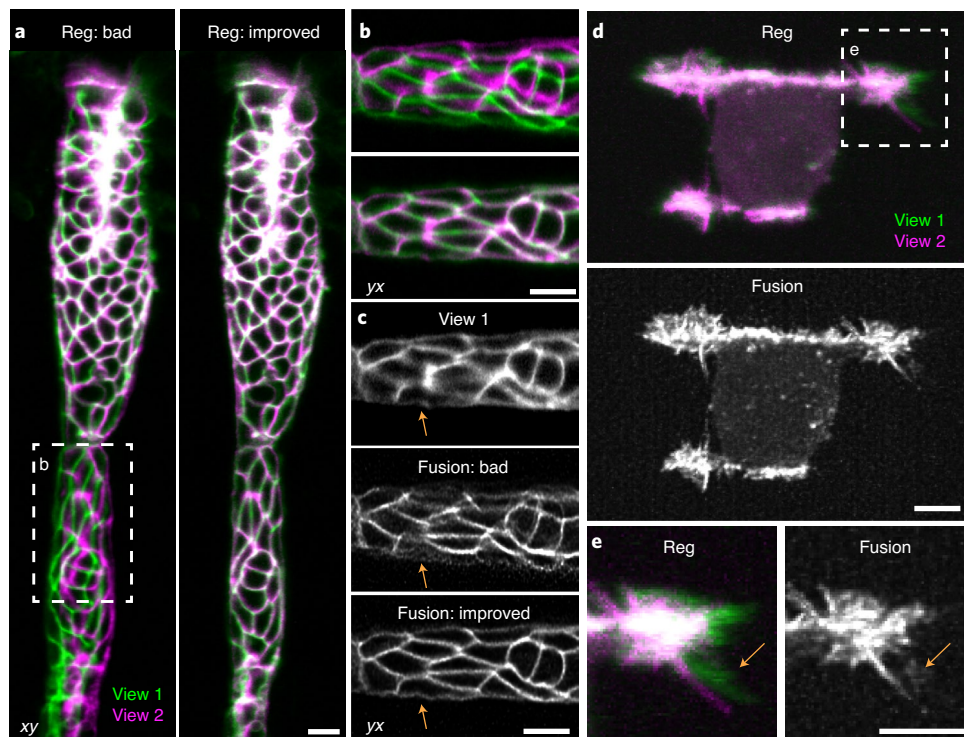


Fig. 6 | Registration failure and motion artifact in multiview fusion. a, Images of zebrafish embryo expressing Lyn-eGFP, showing bad (left) and improved (right) registration on two views. Green and magenta colors indicate the two different views and white color indicates the overlap of the two views. **b**, Higher magnification images of the dashed white box in **a**, with bad (top) and improved (bottom) registration. **c**, Raw (top) and two-view fusion images from bad (middle) and improved (bottom) registration. Note the smeared structures in

the fusion result caused by registration failure (orange arrows). **d**, Registration (top) and two-view fusion (bottom) images of C2C12 cell expressing actin-GFP, showing the motion artifacts introduced by fast local movements within one frame of the multiview acquisition. **e**, Higher magnification images of the dashed white box in **d**, highlighting the motion artifact in registration and fusion (orange arrows). Scale bars, 10 μm in **a–c**, 5 μm in **d** and **e**. Data acquired with diSPIM.

Regardless of the specific implementation, all multiview techniques rely on postprocessing to fuse individual views into a final image^{55,77–79}. In general, postprocessing procedures involve a first step of image registration that transforms the views so that they are spatially co-aligned, and a second step of image fusion to combine the registered views into a single, final image. Registration is essential to the success of subsequent multiview fusion, as suboptimal registration usually leads to noticeable artifacts in the final reconstruction. In practice, imperfect registration may arise for the following reasons.

First, selection of a registration algorithm is crucial. These algorithms come in increasing levels of complexity⁸⁰ depending on the specimen and the microscope optics (Supplementary Fig. 8). In the simplest case, consider a fixed specimen viewed from multiple angles with identical objective lenses. Here, registering each viewpoint requires only (1) rotating one viewpoint to match the other and (2) translating the viewpoints such that they overlap. This registration method is known as a rigid body transformation⁸¹ (Supplementary Fig. 8 top). Unfortunately, the complex and rapidly changing nature of the specimen often renders such simple registration methods ineffective. The next level of complexity is a class of registration methods known as affine transformations. The difference between affine and rigid body transformations is that the former also enables changes in scale and shearing of images⁸⁰ (Supplementary Fig. 8 middle). Therefore, rigid body transformations are a subset of affine transformation. However, the limitation of affine transformations is that they are still linear. That is, a straight line will always remain straight and parallel lines will remain parallel after an affine transformation. There are cases, however, wherein this may not be sufficient; if so, nonlinear transformations may be required (Supplementary Fig. 8 bottom). As the name suggests, nonlinear transformations no longer requiring linearity as

a constraint⁸², thus facilitating local ‘warping’ and distortions that are sometimes required for image registration⁸². In the context of multiview microscopy, one reason for such a complex transform would be the small distortions caused by imperfections in the objective lenses, such as those described earlier. It may at first be tempting to opt for the most complex and comprehensive registration method to ensure the multiple views are properly aligned. Such an approach, however, comes at the cost of computational time and complexity. Moreover, image quantification—in particular, intensity-based quantifications—become increasingly nontrivial with more complex transformations. It is prudent to opt for the least complex method that properly registers the data to best balance accuracy and speed. The success of the registration can be measured and quantified with the NCC, similar to image tiling.

As a demonstration, we imaged a living zebrafish embryo expressing Lyn-eGFP from two orthogonal views on a diSPIM. When registering the two views, we find that a rigid body transformation is insufficient (Figs. 6a left, and 6b top), causing obvious fusion artifacts (Fig. 6c middle). A full affine transformation algorithm, however, is far more successful (Fig. 6a right, Extended Data Fig. 1 bottom), generating a registration of the two volumes such that subsequent fusion lacks obvious artifacts and has near-isotropic resolution (Fig. 6c bottom). The fusion itself can be performed in a variety of ways ranging from simple averaging to, as in this case, more complex methods such as joint deconvolution. We note that deconvolution is frequently a core component of multiview fusion, and thus the caveats described above must be considered when using such methods. Given that an affine transformation appropriately registers the two views, it is not necessary to continue to nonlinear transformations as they would only yield extraneous complexity. An additional practical consideration

is that the individual views themselves may carry too little structural context, making registration based solely on image-content a challenging task. By introducing fiducials (such as beads) that appear in each view, the registration may be performed with an interest point-based algorithm⁷⁷.

Finally, living samples with highly dynamic movements deserve extra scrutiny. A basic assumption in multiview imaging is that different views represent the same underlying structure. If the sample moves during the acquisition, this assumption is violated, potentially resulting in severe artifacts depending on the degree of motion. To demonstrate this effect, we show a dual-view example of live C2C12 cells expressing actin-GFP, captured on a diSPIM. Although the overall cell registers well, the filaments in the right corner (Fig. 6d, dashed white box) move rapidly and do not overlap in the two views. After multiview fusion, artifacts are evident in the vicinity of the filaments (Fig. 6e) but not the rest of the cell (Fig. 6d bottom). The easiest solution to this problem is to image fast enough to adequately sample even the fastest movements, keeping in mind that fine structures need only move by more than the resolution limit in one frame to cause detectable motion blur. If this is not possible, an alternative approach is to seek out a system capable of acquiring multiple views simultaneously rather than sequentially⁸³. If neither situation is plausible, we advise carefully checking the fusion against the raw images, using the latter for quantitative analysis if artifacts are present.

Discussion

A common tenet in physics and mathematics stems from the late Nobel Laureate Maurice Allais, who is quoted as saying ‘a theory is only as good as its assumptions’⁸⁴. This principle holds true across disciplines and methodologies, including fluorescence microscopy. The conclusions we make and theories we draft about biological processes hinge on the assumptions that underly the very microscopy data from which they are derived. We assume the brightness we measure in an image corresponds to protein concentration, and the location of an object in our data accurately represents its position in a specimen. Fundamentally, we presume our images are representative of the true biological structure. Unfortunately, these assumptions are often violated in practice and LSFM is no exception.

LSFM is an attractive microscopy modality for scientists across disciplines. The minimal photobleaching and phototoxicity coupled with enhanced optical sectioning and contrast enables rapid visualization of intricate biological processes over long durations⁸⁵, and numerous length scales^{19,20}. Modern LSFM, however, is a relatively nascent technology. Although conceptually the principle has existed for over a century⁸⁶, its application dates back only three decades¹⁸. Given the lengthy path from technological development to commercialization⁸⁷, modern light sheet microscopes are only recently becoming accessible to most biologists. Unfortunately, there exists a tempting misconception to conflate technological complexity with robustness and trustworthiness⁴. Complex microscopy systems, however, often deserve extra scrutiny when it comes to quantitative analysis.

In this Perspective, we outlined many factors that can undermine quantitative LSFM and provide guidance on proper calibrations and corrections (summarized in Extended Data Fig. 1). It may be daunting, however, to envision tackling each of these considerations for all quantitative LSFM experiments. Thankfully, the gamut of issues we describe are not all applicable to every quantitative metric, and therefore one must only consider and correct for those factors that may influence their specific analyses. For example, morphological characterizations will be relatively insensitive to the uniformity of excitation intensity, although proper flatfield correction may ease segmentation. Similarly, the degradation of light sheet confinement may be of little importance if the biological process of interest occurs, for example, in thin samples or along the most superficial layer of a large specimen. While we have attempted to provide a useful list of

common pitfalls in quantitative LSFM, it is the specific experiment that should dictate which of these factors need to be accounted for to ensure accuracy and reproducibility.

While considering the factors described here will ensure an improved quantitative strategy for LSFM, the struggles in accurately quantifying biological structures and processes do not end with the microscope. More specifically, it should be appreciated that the sample itself can become a source of error in quantitative microscopy⁸⁸. The allure of studying biological processes within their true physiological context has pushed researchers toward imaging deep within specimens. Unfortunately, such imaging is rife with optical aberrations, which in turn compromise image quantification. For example, spatially varying refractive indices within the specimen may alter the position of the light sheet relative to the focal plane. Adaptive optics is an active frontier of research that aims to correct these aberrations through measuring and counteracting the distortions to the wavefront caused by the specimen⁸⁹. Thus, adaptive optics may prove to be a useful tool for quantitative LSFM deeper with biological samples^{90–94}. Unfortunately, adaptive optics is only effective in weakly scattering samples⁹⁰, and thus is predominantly useful in model organisms that are optically transparent. Other systems may be better served by opting for two-photon LSFM^{20,95–98}, either in isolation or combination with adaptive optics.

We have focused this Perspective on LSFM, yet the caution we advise is applicable beyond this single method. We encourage the utmost scrutiny when it comes to quantitative microscopy using any imaging modality. Each method—be it super-resolution microscopy, deep tissue imaging or LSFM—warrants a careful consideration of how the assumptions inherent to quantitative microscopy could be invalidated. The default state of mind should be that of healthy skepticism rather than blind optimism. This principle further applies to computational methods in image analysis and processing. For example, machine learning and artificial intelligence have exceptional promise in image restoration and denoising^{99,100}, which could be a beneficial tool in using LSFM in conjunction with particularly dim or photosensitive samples. It is crucial, however, to understand what assumptions go into these tools and if they hold true for the task at hand. Asking biologists to be aware of each caveat for all microscopy modalities and analysis techniques, however, can be an impractical overreach. It is advisable to rely on local and global resources, such as imaging core facilities, to provide the expertise in performing quantitative microscopy with the latest technologies. This collaboration will inevitably yield more reproducible and robust measurements, and thus improved biological insight.

Data availability

Data used in this article are available at <https://doi.org/10.6084/m9.figshare.c.6211429> or from the authors on request.

References

1. Wait, E. C., Reiche, M. A. & Chew, T. L. Hypothesis-driven quantitative fluorescence microscopy—the importance of reverse-thinking in experimental design. *J. Cell Sci.* **133**, jcs250027 (2020).
2. Esposito, A. et al. Quantitative fluorescence microscopy techniques. *Methods Mol. Biol.* **586**, 117–142 (2009).
3. Waters, J. C. & Wittmann, T. in *Quantitative Imaging in Cell Biology* (eds Waters, J. C. & Wittman, T.) Ch. 1 (Academic Press, 2014).
4. Lecoq, J., Orlova, N. & Grewe, B. F. Wide. Fast. Deep: recent advances in multiphoton microscopy of in vivo neuronal activity. *J. Neurosci.* **39**, 9042–9052 (2019).
5. Stelzer, E. H. K. et al. Light sheet fluorescence microscopy. *Nat. Rev. Methods Prim.* **1**, 73 (2021).
6. Jacquemet, G., Carisey, A. F., Hamidi, H., Henriques, R. & Leterrier, C. The cell biologist’s guide to super-resolution microscopy. *J. Cell Sci.* **133**, jcs240713 (2020).

7. Ji, N. Adaptive optical fluorescence microscopy. *Nat. Methods* **14**, 374–380 (2017).
8. Grimm, J. B. & Lavis, L. D. Caveat fluorophore: an insiders' guide to small-molecule fluorescent labels. *Nat. Methods* <https://doi.org/10.1038/s41592-021-01338-6> (2021).
9. Rodriguez, E. A. et al. The growing and glowing toolbox of fluorescent and photoactive proteins. *Trends Biochem. Sci.* **42**, 111–129 (2017).
10. Lelek, M. et al. Single-molecule localization microscopy. *Nat. Rev. Methods Prim.* **1**, 39 (2021).
11. Combs, C. A. & Shroff, H. Fluorescence microscopy: a concise guide to current imaging methods. *Curr. Protoc. Neurosci.* **2017**, 2.1.1–2.1.25 (2017).
12. Reynaud, E. G., Peychl, J., Huisken, J. & Tomancak, P. Guide to light-sheet microscopy for adventurous biologists. *Nat. Methods* **12**, 30–34 (2014).
13. Royer, L. A., Lemon, W. C., Chhetri, R. K. & Keller, P. J. A practical guide to adaptive light-sheet microscopy. *Nat. Protoc.* **13**, 2462–2500 (2018).
14. Power, R. M. & Huisken, J. A guide to light-sheet fluorescence microscopy for multiscale imaging. *Nat. Methods* **14**, 360–373 (2017).
15. Girkin, J. M. & Carvalho, M. T. The light-sheet microscopy revolution. *J. Optics* **20**, 053002 (2018).
16. Wan, Y., McDole, K. & Keller, P. J. Light-sheet microscopy and its potential for understanding developmental processes. *Annu. Rev. Cell Dev. Biol.* **35**, 655–681 (2019).
17. Huisken, J., Swoger, J., Del Bene, F., Wittbrodt, J. & Stelzer, E. H. K. Optical sectioning deep inside live embryos by selective plane illumination microscopy. *Science* **305**, 1007–1009 (2004).
18. Voie, A. H., Burns, D. H. & Spelman, F. A. Orthogonal-plane fluorescence optical sectioning: three-dimensional imaging of macroscopic biological specimens. *J. Microsc.* **170**, 229–236 (1993).
19. Gebhardt, J. C. M. et al. Single-molecule imaging of transcription factor binding to DNA in live mammalian cells. *Nat. Methods* **10**, 421–426 (2013).
20. Wolf, S. et al. Whole-brain functional imaging with two-photon light-sheet microscopy. *Nat. Methods* **12**, 379–380 (2015).
21. Waters, J. C. Accuracy and precision in quantitative fluorescence microscopy. *J. Cell Biol.* **185**, 1135–1148 (2009).
22. Jonkman, J., Brown, C. M., Wright, G. D., Anderson, K. I. & North, A. J. Tutorial: guidance for quantitative confocal microscopy. *Nat. Protoc.* **15**, 1585–1611 (2020).
23. North, A. J. Seeing is believing? A beginners' guide to practical pitfalls in image acquisition. *J. Cell Biol.* **172**, 9–18 (2006).
24. Lee, J. Y. & Kitaoka, M. A beginner's guide to rigor and reproducibility in fluorescence imaging experiments. *Mol. Biol. Cell* **29**, 1519–1525 (2018).
25. Brown, C. M. Fluorescence microscopy—avoiding the pitfalls. *J. Cell Sci.* **120**, 1703–1705 (2007).
26. Chen, B. C. et al. Lattice light-sheet microscopy: imaging molecules to embryos at high spatiotemporal resolution. *Science* **346**, 1257998 (2014).
27. Keller, P. J., Schmidt, A. D., Wittbrodt, J. & Stelzer, E. H. K. Reconstruction of zebrafish early embryonic development by scanned light sheet microscopy. *Science* **322**, 1065–1069 (2008).
28. Chang, B. J. et al. Universal light-sheet generation with field synthesis. *Nat. Methods* **16**, 235–238 (2019).
29. Self, S. A. Focusing of spherical Gaussian beams. *Appl. Opt.* **22**, 658 (1983).
30. Planchon, T. A. et al. Rapid three-dimensional isotropic imaging of living cells using Bessel beam plane illumination. *Nat. Methods* **8**, 417–423 (2011).
31. Fahrbach, F. O. & Rohrbach, A. A line scanned light-sheet microscope with phase shaped self-reconstructing beams. *Opt. Express* **18**, 24229 (2010).
32. Gao, L. Extend the field of view of selective plan illumination microscopy by tiling the excitation light sheet. *Opt. Express* <https://doi.org/10.1364/oe.23.006102> (2015).
33. Dean, K. M., Roudot, P., Welf, E. S., Danuser, G. & Fiolka, R. Deconvolution-free subcellular imaging with axially swept light sheet microscopy. *Biophys. J.* **108**, 2807–2815 (2015).
34. Kim, B. et al. Open-top axially swept light-sheet microscopy. *Biomed. Opt. Express* **12**, 2328 (2021).
35. Liu, Y., Rollins, A. M. & Jenkins, M. W. CompassLSM: axially swept light-sheet microscopy made simple. *Biomed. Opt. Express* **12**, 6571 (2021).
36. Landry, J., Hamann, S. & Solgaard, O. High-speed axially swept light sheet microscopy using a linear MEMS phased array for isotropic resolution. *J. Biomed. Opt.* **25**, 106504 (2020).
37. Chakraborty, T. et al. Light-sheet microscopy of cleared tissues with isotropic, subcellular resolution. *Nat. Methods* <https://doi.org/10.1038/s41592-019-0615-4> (2019).
38. Wu, Y. et al. Spatially isotropic four-dimensional imaging with dual-view plane illumination microscopy. *Nat. Biotechnol.* **31**, 1032–1038 (2013).
39. Kumar, A. et al. Dual-view plane illumination microscopy for rapid and spatially isotropic imaging. *Nat. Protoc.* **9**, 2555–2573 (2014).
40. Octave, J. -N., Schneider, Y. -J., Trouet, A. & Crichton, R. R. Transferrin uptake by cultured rat embryo fibroblasts: the influence of temperature and incubation time, subcellular distribution and short-term kinetic studies. *Eur. J. Biochem.* **115**, 611–618 (1981).
41. Tsien, R. Y., Ernst, L. & Waggoner, A. in *Handbook of Biological Confocal Microscopy* 3rd edn (ed. Pawley, J. B.) 338–352 (Springer, 2006).
42. Gavryusev, V. et al. Dual-beam confocal light-sheet microscopy via flexible acousto-optic deflector. *J. Biomed. Opt.* **24**, 106504 (2019).
43. Glaser, A. K. et al. Multidirectional digital scanned light-sheet microscopy enables uniform fluorescence excitation and contrast-enhanced imaging. *Sci. Rep.* **8**, 13878 (2018).
44. G. De, Medeiros et al. Confocal multiview light-sheet microscopy. *Nat. Commun.* **6**, 8881 (2015).
45. Baumgart, E. & Kubitschek, U. Scanned light sheet microscopy with confocal slit detection. *Opt. Express* **20**, 21805 (2012).
46. Chakraborty, T. et al. Light-sheet microscopy of cleared tissues with isotropic, subcellular resolution. *Nat. Methods* **16**, 1109–1113 (2019).
47. Shutova, M. S. & Svitkina, T. M. Common and specific functions of nonmuscle myosin II paralogs in cells. *Biochemistry (Mosc.)* <https://doi.org/10.1134/S0006297918120040> (2018).
48. Kask, P., Palo, K., Hinnah, C. & Pommerencke, T. Flat field correction for high-throughput imaging of fluorescent samples. *J. Microsc.* <https://doi.org/10.1111/jmi.12404> (2016).
49. Smith, K. et al. CIDRE: an illumination-correction method for optical microscopy. *Nat. Methods* <https://doi.org/10.1038/nmeth.3323> (2015).
50. Likar, B., Maintz, J. B. A., Viergever, M. A. & Pernuš, F. Retrospective shading correction based on entropy minimization. *J. Microsc.* <https://doi.org/10.1046/j.1365-2818.2000.00669.x> (2000).
51. Tomer, R., Khairy, K., Amat, F. & Keller, P. J. Quantitative high-speed imaging of entire developing embryos with simultaneous multiview light-sheet microscopy. *Nat. Methods* **9**, 755–763 (2012).
52. Huisken, J. & Stainier, D. Y. R. Even fluorescence excitation by multidirectional selective plane illumination microscopy (mSPIM). *Opt. Lett.* **32**, 2608 (2007).

53. Ricci, P. et al. Removing striping artifacts in light-sheet fluorescence microscopy: a review. *Prog. Biophys. Mol. Biol.* **168**, 52–65 (2022).
54. Gao, R. et al. Cortical column and whole-brain imaging with molecular contrast and nanoscale resolution. *Science* **363**, eaau8302 (2019).
55. Guo, M. et al. Rapid image deconvolution and multiview fusion for optical microscopy. *Nat. Biotechnol.* **38**, 1337–1346 (2020).
56. Ueda, H. R. et al. Whole-brain profiling of cells and circuits in mammals by tissue clearing and light-sheet microscopy. *Neuron* **106**, 369–387 (2020).
57. Voigt, F. F. et al. The mesoSPIM initiative: open-source light-sheet microscopes for imaging cleared tissue. *Nat. Methods* **16**, 1105–1108 (2019).
58. Chen, F., Tillberg, P. W. & Boyden, E. S. Expansion microscopy. *Science* **347**, 543–548 (2015).
59. Chung, K. et al. Structural and molecular interrogation of intact biological systems. *Nature* **497**, 332–337 (2013).
60. Dodt, H. U. et al. Ultramicroscopy: three-dimensional visualization of neuronal networks in the whole mouse brain. *Nat. Methods* **4**, 331–336 (2007).
61. Hama, H. et al. ScaleS: an optical clearing palette for biological imaging. *Nat. Neurosci.* **18**, 1518–1529 (2015).
62. Jing, D. et al. Tissue clearing of both hard and soft tissue organs with the pegasos method. *Cell Res.* **28**, 803–818 (2018).
63. Renier, N. et al. IDISCO: a simple, rapid method to immunolabel large tissue samples for volume imaging. *Cell* **159**, 896–910 (2014).
64. Susaki, E. A. et al. Whole-brain imaging with single-cell resolution using chemical cocktails and computational analysis. *Cell* **157**, 726–739 (2014).
65. Tainaka, K., Kuno, A., Kubota, S. I., Murakami, T. & Ueda, H. R. Chemical principles in tissue clearing and staining protocols for whole-body cell profiling. *Annu. Rev. Cell Dev. Biol.* **32**, 713–741 (2016).
66. Preibisch, S., Saalfeld, S. & Tomancak, P. Globally optimal stitching of tiled 3D microscopic image acquisitions. *Bioinformatics* **25**, 1463–1465 (2009).
67. Burger, W. & Burge, M. *Principles of Digital Image Processing: Advanced Methods. Principles of Digital Image Processing* (Springer, 2013).
68. Pitas, I. *Digital Image Processing Algorithms and Applications* (Wiley, 2000).
69. Wallace, W., Schaefer, L. H. & Swedlow, J. R. A workingperson's guide to deconvolution in light microscopy. *BioTechniques* <https://doi.org/10.2144/01315bi01> (2001).
70. Biggs, D. S. C. A practical guide to deconvolution of fluorescence microscope imagery. *Micros. Today* <https://doi.org/10.1017/s1551929510991311> (2010).
71. McNally, J. G., Karpova, T., Cooper, J. & Conchello, J. A. Three-dimensional imaging by deconvolution microscopy. *Methods* <https://doi.org/10.1006/meth.1999.0873> (1999).
72. Aaron, J. & Chew, T. L. A guide to accurate reporting in digital image processing—can anyone reproduce your quantitative analysis? *J. Cell Sci.* <https://doi.org/10.1242/jcs.254151> (2021).
73. Pitrone, P. G. et al. OpenSPIM: an open-access light-sheet microscopy platform. *Nat. Methods* **10**, 598–599 (2013).
74. Swoger, J., Verveer, P., Greger, K., Huisken, J. & Stelzer, E. H. K. Multi-view image fusion improves resolution in three-dimensional microscopy. *Opt. Express* **15**, 8029 (2007).
75. Krzic, U., Gunther, S., Saunders, T. E., Streichan, S. J. & Hufnagel, L. Multiview light-sheet microscope for rapid in toto imaging. *Nat. Methods* **9**, 730–733 (2012).
76. Chhetri, R. K. et al. Whole-animal functional and developmental imaging with isotropic spatial resolution. *Nat. Methods* **12**, 1171–1178 (2015).
77. Preibisch, S., Saalfeld, S., Schindelin, J. & Tomancak, P. Software for bead-based registration of selective plane illumination microscopy data. *Nat. Methods* **7**, 418–419 (2010).
78. Amat, F. et al. Efficient processing and analysis of large-scale light-sheet microscopy data. *Nat. Protoc.* **10**, 1679–1696 (2015).
79. Preibisch, S. et al. Efficient Bayesian-based multiview deconvolution. *Nat. Methods* **11**, 645–648 (2014).
80. Brown, L. G. A survey of image registration techniques. *ACM Comput. Surv.* **24**, 325–376 (1992).
81. Ashburner, J. & Friston, K. in *Human Brain Function* 2nd edn (eds Friston, K. et al.) 635–653 (Elsevier, 2003).
82. Ruthotto, L. & Modersitzki, J. in *Handbook of Mathematical Methods in Imaging* 2nd edn, Vol. 1 (ed. Scherzer, O.) 2005–2051 (Springer, 2015).
83. Wu, Y. et al. Reflective imaging improves spatiotemporal resolution and collection efficiency in light sheet microscopy. *Nat. Commun.* **8**, 1452 (2017).
84. Allais, M. *L'anisotropie de l'espace: la nécessaire révision de certains postulats des théories contemporaines. Les données de l'expérience* (Clément Juglar, 1997).
85. Royer, L. A. et al. Adaptive light-sheet microscopy for long-term, high-resolution imaging in living organisms. *Nat. Biotechnol.* **34**, 1267–1278 (2016).
86. Siedentopf, H. & Zsigmondy, R. Über Sichtbarmachung und Größenbestimmung ultramikroskopischer Teilchen, mit besonderer Anwendung auf Goldrubingläser. *Ann. Phys.* **315**, 1–39 (1902).
87. Chew, T.-L., George, R., Soell, A. & Betzig, E. Opening a path to commercialization. *Opt. Photonics N.* **28**, 42 (2017).
88. Reiche, M. A. et al. When light meets biology: how the specimen affects quantitative microscopy. *J. Cell Sci.* **135**, jcs259656 (2022).
89. Hampson, K. M. et al. Adaptive optics for high-resolution imaging. *Nat. Rev. Methods Prim.* **1**, 68 (2021).
90. Liu, T. L. et al. Observing the cell in its native state: imaging subcellular dynamics in multicellular organisms. *Science* **360**, eaaq1392 (2018).
91. Hubert, A. et al. Adaptive optics light-sheet microscopy based on direct wavefront sensing without any guide star. *Opt. Lett.* **44**, 2514 (2019).
92. Wilding, D., Pozzi, P., Soloviev, O., Vdovin, G. & Verhaegen, M. Adaptive illumination based on direct wavefront sensing in a light-sheet fluorescence microscope. *Opt. Express* **24**, 24896 (2016).
93. Bourgenot, C., Saunter, C. D., Taylor, J. M., Girkin, J. M. & Love, G. D. 3D adaptive optics in a light sheet microscope. *Opt. Express* **20**, 13252 (2012).
94. Schoeneberg, J. 4D cell biology: adaptive optics lattice light-sheet imaging and AI powered big data processing of live stem cell-derived organoids. *J. Biomol. Tech.* **31**, S33 (2020).
95. Mahou, P., Vermot, J., Beaufort, E. & Supatto, W. Multicolor two-photon light-sheet microscopy. *Nat. Methods* **11**, 600–601 (2014).
96. Truong, T. V., Supatto, W., Koos, D. S., Choi, J. M. & Fraser, S. E. Deep and fast live imaging with two-photon scanned light-sheet microscopy. *Nat. Methods* **8**, 757–762 (2011).
97. Zong, W. et al. Large-field high-resolution two-photon digital scanned light-sheet microscopy. *Cell Res.* **25**, 254–257 (2015).
98. Escobet-Montalbán, A. et al. Three-photon light-sheet fluorescence microscopy. *Opt. Lett.* **43**, 5484 (2018).
99. Weigert, M. et al. Content-aware image restoration: pushing the limits of fluorescence microscopy. *Nat. Methods* **15**, 1090–1097 (2018).

100. Krull, A., Vičar, T., Prakash, M., Lalit, M. & Jug, F. Probabilistic Noise2Void: unsupervised content-aware denoising. *Front. Comput. Sci.* <https://doi.org/10.3389/fcomp.2020.00005> (2020).

Acknowledgements

We thank S. Khuon, L. Eisenman, A. Nain, C. Hernandez-Padilla and L. Zhang for cell culture and sample preparation; W. Lemon for preparation of *D. melanogaster* embryos; D. Dalle Nogare and A. Chitnis for preparation of zebrafish samples; R. Christensen for *C. elegans* sample preparation; Z. Bao for providing the OD58 *C. elegans* strain; Y. Su, I. Curtin, F. Kyere, J. Stein and M.S. Itano for advice and assistance with brain sample preparation; and M. DeSantis and the Janelia Light Microscopy Facility. This work was supported in part by the intramural research program of the National Institute of Biomedical Imaging and Bioengineering at the National Institutes of Health (M.G., H.D.V., Y.W. and H.S.). The Advanced Imaging Center at Janelia Research Campus was generously supported by the Howard Hughes Medical Institute and the Gordon and Betty Moore Foundation (C.M.H. and T.-L.C.).

Author contributions

C.M.H., M.G., H.D.V. and Y.W. performed the imaging experiments and accompanying analyses. H.S. and T.-L.C. oversaw the project. All authors contributed to writing and editing the manuscript.

Competing interests

The authors declare no competing interests.

Additional information

Extended data is available for this paper at <https://doi.org/10.1038/s41592-022-01632-x>.

Supplementary information The online version contains supplementary material available at <https://doi.org/10.1038/s41592-022-01632-x>.

Correspondence should be addressed to Teng-Leong Chew.

Peer review information *Nature Methods* thanks Kevin Dean, Niall Geoghegan, and the other, anonymous, reviewer(s) for their contribution to the peer review of this work. Primary Handling Editor: Rita Strack, in collaboration with the *Nature Methods* team.

Reprints and permissions information is available at www.nature.com/reprints.

Publisher's note Springer Nature remains neutral with regard to jurisdictional claims in published maps and institutional affiliations.

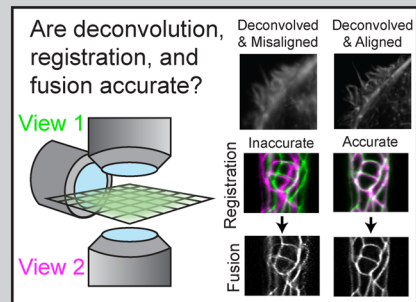
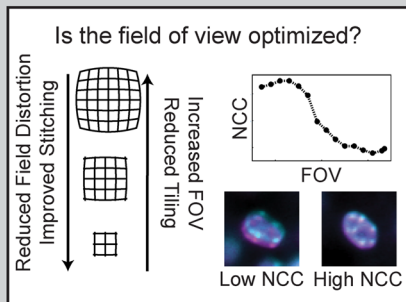
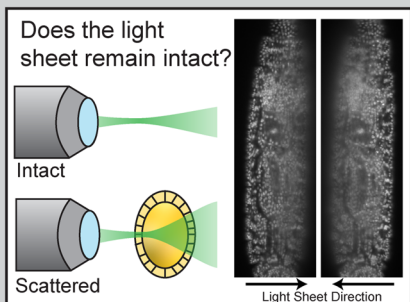
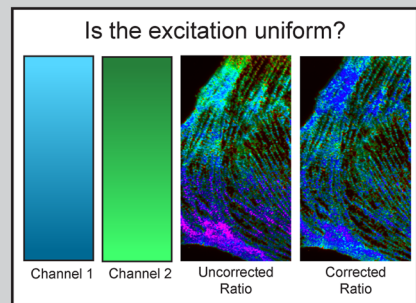
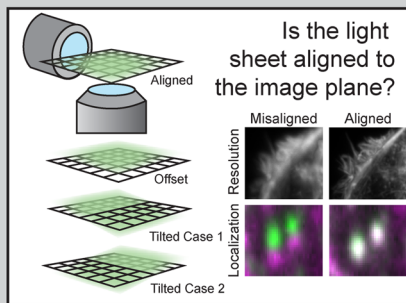
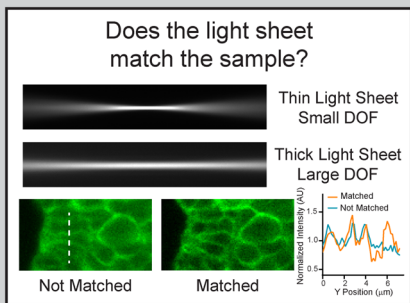
Springer Nature or its licensor holds exclusive rights to this article under a publishing agreement with the author(s) or other rightsholder(s); author self-archiving of the accepted manuscript version of this article is solely governed by the terms of such publishing agreement and applicable law.

© Springer Nature America, Inc. 2022

Practical Considerations for Quantitative Light Sheet Fluorescence Microscopy



Chad M. Hobson, Min Guo, Harshad D. Vishwasrao, Yicong Wu, Hari Shroff, Teng-Leong Chew



Extended Data Fig. 1 | ‘Practical Considerations for Quantitative Light Sheet Fluorescence Microscopy’ Infographic. Summary of the important considerations for quantitative LSM described in this Perspective.